Iraqi Journal of Veterinary Sciences

www.vetmedmosul.com

Fluorescent imaging and bio-cellular uptake assessment of gold-near infrared dye conjugated cockle shell calcium carbonate nanoparticles

H.K. Kiranda[1], R.B. Mahmud[2], S.K. Mahmood[3] and Z.A. Zakaria[4]

[1]Research and Innovation Center, Humber College, Institute of Technology and Advanced Learning, Toronto, Ontario, Canada, [2]Department of Imaging, Faculty of Medicine and Health Sciences, University of Putra Malaysia, Serdang, Malaysia, [3]Department of Anatomy, College of Veterinary Medicine, University of Mosul, Mosul, Iraq, [4]Department of Veterinary Preclinical Sciences, Faculty of Veterinary Medicine, University of Putra Malaysia, Serdang, Malaysia

Article information

Article history:
Received 11 February, 2024
Accepted 30 June, 2024
Published online 16 September, 2024

Keywords:
Aragonite
Au, Bio-cellular
Fluorescent microscope
Nanoparticles

Correspondence:
S.K. Mahmood
saffanhjeber@uomosul.edu.iq

Abstract

In recent years, fluorescent imaging has emerged as an active area of interest in medical imaging. Fluorescent imaging plays a critical role in molecular imaging. Evidence suggests its use in providing a detailed structural outlook and genetic and cellular operatives of the body procedures on a molecular plane. Imaging agents are identified to be related to risks such as not biologically disintegration and great poisonousness. Researchers have shown a keen attentiveness to the growth of targeted multifunctional agents in oncology and near-infrared (NIR) fluorescence imaging. This study assessed fluorescent imaging and bio-cellular acceptance of the gold (NIR) conjugated cockle shell-derived calcium carbonate nanoparticles Au-CsCaCO3NPs. The synthesized Au-CsCaCO3NPs were characterized by Transmission electron microscopy (TEM) for size and morphology, Zeta potential, and UV-Vis spectrophotometer. Biocompatibility of Au-CsCaCO3NPs in cultured human breast carcinoma cells MCF-7 and mouse embryonic fibroblast cells NIH3T3 was evaluated using bioassays like Lactate Dehydrogenase LDH and Reactive Oxygen Species ROS for toxic examination. Cellular morphology and uptake were studied by fluorescence and confocal microscopy. The outcomes proved that MCF-7 treated Au-CsCaCO3NP cells observed more cell deaths than NIH3T3 treated Au-CsCaCO3NP cells. Additionally, the cells were capable of assuming nanoparticles within their cellular compartments. In conclusion, gold-near infrared dye conjugated cockle shell calcium carbonate nanoparticles Au-CsCaCO3NPs were easily synthesized, biocompatible, and environmentally friendly. It is safe to state that the Au-CsCaCO3NPs could be used for imaging and could present opportunities for progressing cancer imaging.

DOI: 10.33899/ijvs.2024.146804.3470,

Introduction

In current years, the use of nanoparticles (NPs) has been noted with confined diameter size ranging from 10-100 nm (1) and has also created great promise with their use in biomedical photo-imaging, recovering medication, scaffolds studies, drug distribution, therapeutics, and tissue manufacturing (2-14). The last decade has seen a growing trend towards using nanoparticles for imaging (15,16). A considerable amount of literature is being focused on the theme of biogenic nanoparticles such as aragonite calcium carbonate nanoparticles (17) and gold nanoparticles AuNPs (18). Aragonite is a unique of the polymorphs of $CaCO_3$ that naturally and richly exists (95 - 98 %) in (*Anadara granosa*), a mollusc's cockle shell that commonly originates in Malaysia (19). The effects of using calcium carbonate

nanoparticles for imaging have been described with the Eu^{3+}-doped calcium carbonate cubic nanoparticles produced by the carbonation synthetic route and the photoluminescence properties characterized by scanning electron microscope and x-ray diffractometer (20-22). In other related studies, it has been demonstrated that the technique used to develop fabricated oxygen-sensitive polymer nanocapsules using layer-by-layer (LBL) tactic using vaterite calcium carbonate nanoparticles as templates. Additionally, the buffer used was decisive in preserving their reliability and ensuring the nanoparticles were stable in alkaline sodium hydrogen carbonate (23). In addition, it also found that the nanoparticles revealed thermal stability and a notable adsorption capacity caused by vigorous spots like the amino and carbonyl groups (24-26). Regarding the AuNPs, there is a relatively small body of literature concerned with the development of AuNPs bioconjugates and their potential use in imaging or other biomedical applications (27,28). Also, due to their low or non-significant toxicity, they are increasingly used in diagnosis, therapeutics, disease treatment, and targeted drug delivery systems (29-34). In addition, AuNPs bioconjugates maintain high stability upon interaction with biomolecules such as proteins and antibodies (35,36). Major attention is on the AuNP surface plasmon resonance property, which focuses on designing diagnostic biomaterials, drug-targeting agents, therapeutics, and contrast agents (37-43). Furthermore, existing works on AuNPs and their conjugates have extensively been employed in agriculture to enhance the visual detection of pesticides, the food industry to detect contaminants, and the extension of food shelf life (44,45). However, recent developments in biomedical imaging have caused limitations with the imaging probes meant for clinical usage. These include no biological disintegration or gentle elimination and great poisonousness, perplexing the manufacture of a robust imaging indicator, compromising their further evolution into clinical use (15). In addition, research investigations suggest that there are also several challenges associated with targeted tumor nanoparticles administered by intravenous route due to interaction with an intricate atmosphere (46). These include clearance of targeted nanoparticles by the phagocytes, either by effectively removing nanoparticles from circulation, leaving a trivial portion at the tumor sites, or by long retention of the nanoparticles, potentially developing into complications like toxicity (47). Secondly, tumor physiological properties like antigen expression and tumor permeability stop the buildup of nanoparticles or drug delivery in the region (48-50). It has also been elaborated in a prior study that nanoparticles in blood circulation habitually bind to plasma proteins (opsonization) that are phagocyted within the blood, spleen, bone marrow, and liver (51). Similar studies have shown techniques that alleviate these limitations by embracing the stabilization of particle dispersions using coatings and understanding the outcome of the nanoparticles in the bloodstream and their physiochemical properties; thus, there is a substantial need to produce biocompatible nanoparticles with ideal features (52-54). Herewith, Au-CsCaCO3NPs are prepared and assessed *in vitro* using Lactate Dehydrogenase LDH and Reactive Oxygen Species ROS assays. Cellular uptake of the Au-CsCaCO3NPs was evaluated using fluorescence and confocal microscopy. Primarily, the Au-$CsCaCO_3$NPs development is prompted by the need for cost-efficient and biocompatible nanomaterial for imaging. The preparation utilizes method-friendly approaches such as the classic Turkevich method (55) and dodecyl dimethyl betaine (BS -12). The Au-$CsCaCO_3$NP's potential use for fluorescent imaging is also elaborately discussed.

This work aims to evaluate the gold-near infrared dye conjugated cockle shell calcium carbonate nanoparticles through bio-cellular uptake, and confocal and fluorescence imaging.

Materials and Methods

Ethical approval

The work procedure was permitted via IACUC UPM; AUPR015/2015.

Materials and chemicals

The gold colloid solution was bought from Malaysia (Prima Nexus Sdn Bhd). The breast cancer cell line (JCRB: MCF-7) and the fibroblast cell line (JCRB: NIH-3T3) were commercially bought from the Japanese Collection Research Bioresource (JCRB). All other materials and chemicals used were purchased from (Sigma-Aldrich (in Steinheim, Germany, and (USA); Naclai tesque, Inc., Kyoto, Japan; and Cell Biolabs, Inc., San Diego, CA, USA). Incorporation of NIR dye and production of Au-CsCaCO3NPs, characterization of Au-CsCaCO3NPs through Transmission Electron Microscope (TEM), zeta potential and measurement size distribution, UV-VIS spectrophotometer and cell biocompatibility were discussed in (56).

Cells seeding and treatment

The cultured flasks' cells were detached using trypsin and seeded into ninety-six well sterile dishes at a concentration of 1×10^5 cells each well. The ninety-six well dishes were then placed into the 5% carbon dioxide incubator at 37˚C for 24 hours. The media in the wells was aspirated, and the cells were treated and co-cultured in replicates with Au-$CsCaCO_3$NPs solution (concentration of one mg/ml in ten percent serum-free DMEM media), for twenty-four hours, forty-eight hours, and seventy-two hours. The following treatment experience was finished, and the media in the wells was removed and splashed with phosphate-buffered saline. Earlier, it was exchanged with additional media previous to additional new treatments, for example, LDH Assay (57) and ROS Assay (58).

Lactate dehydrogenase assay LDH

Subsequently, cell seeding of MCF-7 cells and NIH3T3 cells in ninety-six-well dishes and treatment, the dishes were incubated for 72 hours after treatment with different concentrations in µg (100, 50, and Control) of the nanoparticle solutions. The 96-well plates were cleared of all previous media, and cell membrane integrity was assessed (58). The protocol measures the amount of LDH out through the lysed cells directly related to the damaged cells.

Lactate dehydrogenase treatment protocol

The 96-well plates were removed from the incubator with the previous treatment. Sterile water and Triton X-100 provided were supplementary to individual wells in triplicates for the pre-seeded and treated plates. The dishes were incubated for ten minutes in a room environment. Approximately 90 µl of media was carefully transferred from each well to clean 96-well plates suitable for micro-plate readers. Around 10 µl of LDH assay reagent was supplementary to the wells and permitted to incubate for 1 hour to allow for LDH activity of the cells. After incubation, the dishes were positioned on a shaker for 10 minutes. The suspension's visual concentration was examined with a micro-plate reader at a wavelength of 450 nanometers; the values were recorded, and a graph was plotted with Excel.

Reactive oxygen species assay ROS

This part of the study was achieved using a protocol from the ROS assay kit. For the preparation of reagents, 1X DCF-DA (20X DCF-DA stock solution was diluted to 1x in serum-free DMEM media and mixed uniformly using a sonicator vortex), and Hydrogen Peroxide (H_2O_2) dilutions were prepared in DMEM serum-free media. For the preparation of a typical curve**,** about one to ten serial dilutions of DCF standards were prepared in a concentration variety of zero µM to ten µM by attenuating the one mM DCF stock in DMEM serum-free media. Approximately 75 µl of individual DCF standard was transferred to a ninety-six-well dish appropriate for fluorescence measurement, followed by 75 µl of the 2X cell lysis buffer. Fluorescence data readings were obtained using a fluorescence microplate reader, measured at 480 nanometres excitation and 530 nanometres secretion.

DCF Dye filling

The 96-well plates were cleared of all previous media and washed well with PBS twice. About 100 µl of 1X DCF-DA prepared solution was supplementary to the cells and incubated for 45-60 min at 37°C. The 96-well dishes were cleared of all solutions and washed away well with PBS twice. The DCF-DA-loaded cells were treated with the prepared hydrogen peroxide in 100 µl media.

Quantitation of Fluorescence

After treatment with the oxidant, the 96-well plates were cleared of all previous media and washed well with PBS twice. About 100 µl of media was supplementary to individually well along with 100 µl of 2X cell lysis buffer, which was carefully miscellaneous and then incubated for 10 minutes. Around 150 µl of the combination was then moved into a hygienic ninety-six-well dish for fluorescent measurement. The fluorescence was documented at 480 nm excitation and 530 nm emission with a fluorescent micro-plate reader. The experiment was conducted in triplicates.

***In-vitro* imaging and cellular acceptance of Au-$CsCaCO_3$NPs**

Breast cancer cells MCF-7 were seeded into six-well dishes and permitted to cultivate in 100% DMEM media. Upon accomplishment 80% cell confluence, the media was removed and then exchanged with 1ml of new culture media complemented with 25 mM HEPES comprising Au-$CsCaCO_3$NPs suspension and incubated at 37˚C for 6 hours. The cells were splashed in PBS solution (3) periods before fluorescent and confocal microscopy examination. Fluorescence images were documented to quantify conjugate nanomaterial uptake by the cells, and fluoresce emission was visualized using a fluorescent microscope (Immunofluorescence microscopy system, Tokyo, Japan).

Fluorescent preparation protocol

The cells were seeded onto four well-chambered sterilized slides (SPL Life sci, made in Korea) and incubated for twenty-four hours overnight. The medium in the wells was detached, and the cells were treated and co-cultured in replicates with Au-$CsCaCO_3$NPs solution for 72 hours. Once the treatment experience was accomplished, the medium in the wells was removed and splashed with PBS twice. The cells were re-suspended after trypsinization, and 0.5 ml of Devil's stain (Acridine Orange (AO) and Propidium Iodide (PI) in the ratio of 1:1) was supplementary to individually well for 60 minutes in a room environment. Afterward, a drop was placed on a clean slide with the coverslip. The slides were examined using fluorescence microscopy (Immunofluorescence microscopy system, Tokyo, Japan).

Confocal preparation protocol

The cells were seeded onto 4-wells chambered sterile slides (SPL life sci, made in Korea) and incubated for twenty-four hours overnight. The medium in the wells was detached, and the cells were treated and co-cultured in replicates with Au-$CsCaCO_3$NPs for 72 hours. Once the treatment experience was accomplished, the medium in the wells was removed and splashed with PBS twice. The cells were stable in 3.7% pre-cooled paraformaldehyde in a room environment for fifteen minutes and afterward splashed twice with PBS. Around 500 µl of Devil's stain was supplementary to individually well for 60 minutes at room

temperature and afterward splashed with PBS twice, followed by the counter stain of 50 µl prepared intermediate DAPI (4', 6-diamidino-2-phenylindole) for two mins at room environment. The wells were finally splashed thrice with PBS in the dark, and coverslips were mounted with Prolong gold antifade reagent (Molecular probe, USA). The slides were finally studied using a confocal laser scanning microscope (Zeiss, Germany).

Statistical examination

All data examination was achieved by SPSS software (Version 10, Chicago, USA) by student's t-test and one-way ANOVA and stated as Mean ± Standard deviation. The level of statistical consequence was P<0.05.

Results

Lactate dehydrogenase assay LDH

This analysis was further intended to evaluate the cell membrane integrity of MCF-7 cell line and NIH3T3 cell line treated with the synthesized Au-CsCaCO3NPs. Analyzing LDH levels after exposure to the concentrations in µg (100, 50, and Control) designed from the assay dose-response for 72 hours. The findings displayed in figure 1 validate that the LDH percentage release of MCF-7 cells treated with Au-$CsCaCO_3$NPs was slightly more significant than that of the Au-$CsCaCO_3$NPs treated NIH3T3 cells.

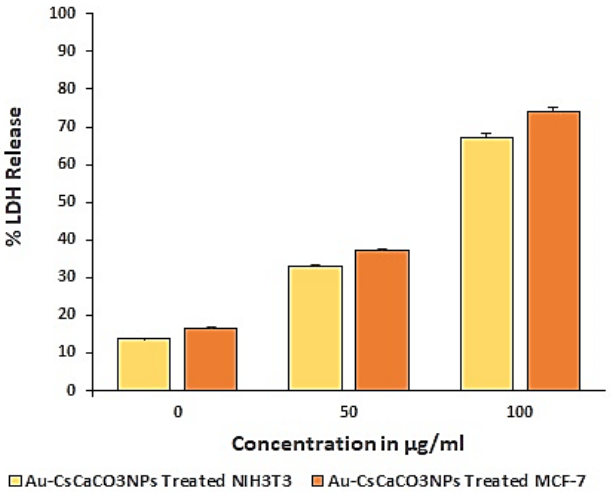

Figure 1: Comparative LDH released by Au-CsCaCO3NPs treated MCF-7 cells and Au-CsCaCO3NPs treated NIH3T3 cells, presenting higher LDH % release with MCF-7 as compared to NIH3T3 at P< 0.05.

Reactive oxygen species ROS

The objective of ROS experimental assay analysis was to further investigate the ROS of Au-CsCaCO3NPs on MCF-7 and NIH3T3 by measuring the relative fluorescence units (RFU) (Figure 2).

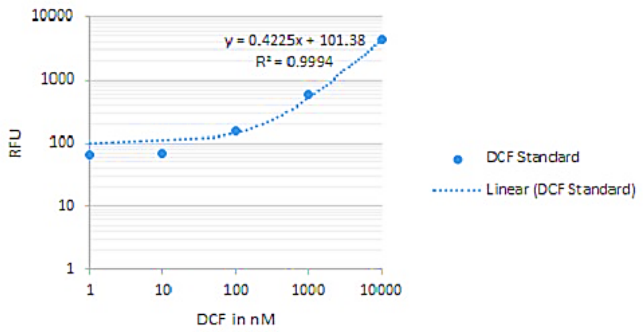

Figure 2: DCF Standard curve.

The results show that Au-$CsCaCO_3$NPs treated MCF-7 cells also showed greater ROS release as matched to the Au-$CsCaCO_3$NPs treated NIH3T3 cells. They displayed minimal ROS release of less than 400 RFU at a concentration of 100 µg in matched to their MCF-7 counterparts (Figure 3).

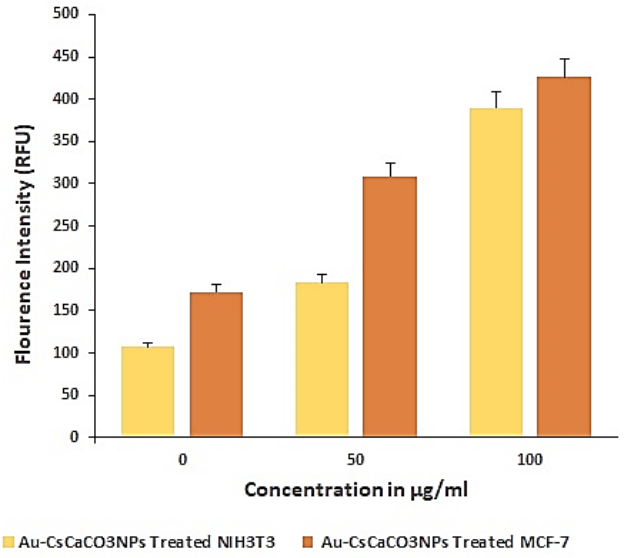

Figure 3: Comparative ROS generation by Au-CsCaCO3NPs treated MCF-7 cells and Au-CsCaCO3NPs treated NIH3T3 cells, presenting higher ROS generation with MCF-7 as compared to NIH3T3 at P<0.05.

Fluorescent imaging and confocal imaging

The purpose of fluorescent and confocal imaging of MCF-7 and NIH3T3 was to morphologically visualize cell death and the possibility of cellular uptake of the nanoparticles using the AO and PI double staining method and DAPI. The results in the MCF-7 fluorescent micrographs display most live cells with the Control, unlike the Au-$CsCaCO_3$NP treated cells, which show more cell death (Figure 4). The NIH3T3 fluorescent micrographs show more live cells with the Control and Au-$CsCaCO_3$NPs (Figure 5).

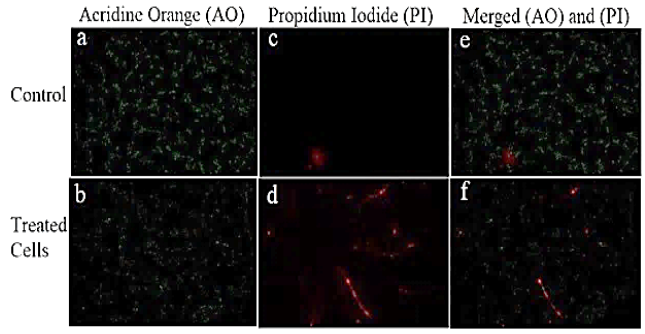

Figure 4: Fluorescent images of MCF-7 cells subsequent treatment with (AO), (PI), and merged (PI and AO). Images (a) and (b) show live cells' subsequent treatment with (AO), with the Control having extra cells equal to Au-CsCaCO3NPs treated cells. Images (c) and (d) show dead cells in the next treatment with (PI), with the Control having fewer cells equal to Au-CsCaCO3NPs treated cells. Images (e) and (f) show live and dead cells together after merging. (Magnification ×10, scale bar 100 µm).

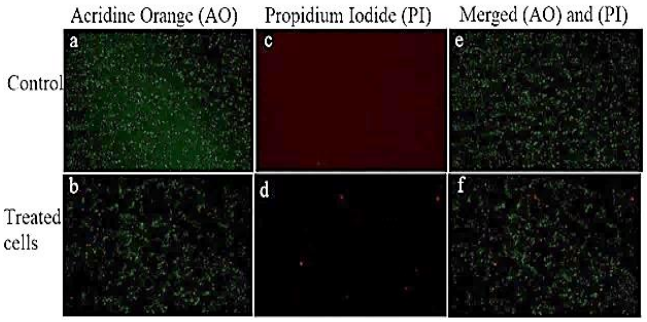

Figure 5: Fluorescent images of NIH3T3 cells next treatment with (AO), (PI), and merged (PI and AO). Images (a) and (b) show live cells next treatment with AO, Au-CsCaCO3NPs treated cells showing not much difference with the Control. Images (c) and (d) show fewer or no dead cells in the next treatment with PI. Images (e) and (f) show live and dead cells together after merging. (Magnification ×10, scale bar 100 µm).

However, the most interesting fact is that the MCF-7 treated cells observed more cell deaths than the NIH3T3 treated cell counterparts. The findings in the confocal micrographs are an overview of the mechanisms of intracellular uptake by MCF-7 and NIH3T3 which show the appearance of the nanoparticles inside the cellular compartment under four different fluorescent filters (blue, green, red, and merged filters) unlike the controls as indicated by arrows within their figures illustrated in figures 6-9.

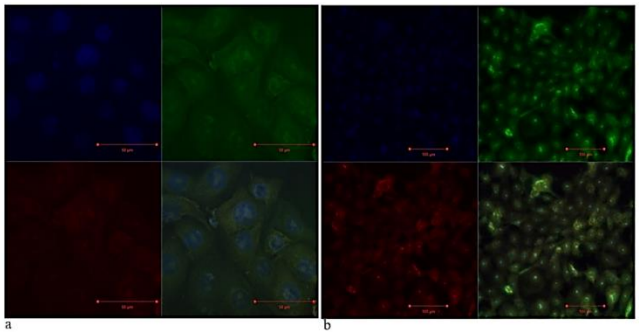

Figure 6: Confocal micrographs of MCF-7 Control presentation cellular morphology under different fluorescent filters using DAPI (blue), AO (green), PI (red), and merged filter. ((A) ×63, scale bar 50 µm (B) ×20, scale bar 100 µm).

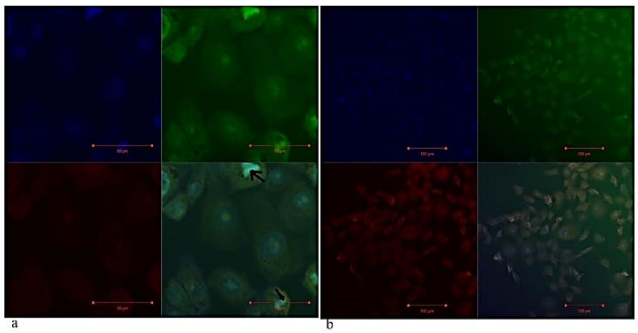

Figure 7: Confocal micrographs of Au-CsCaCO3NPs treated MCF-7 cells presentation cellular acceptance and morphology under different fluorescent filters using DAPI (blue), AO (green), PI (red) and merged filter (living cells (control cells) pointer by black arrows). ((A) ×63, scale bar 50 µm (B) ×20, scale bar 100 µm).

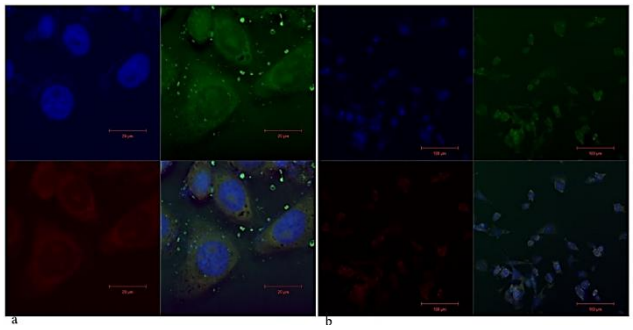

Figure 8: Confocal micrographs of NIH3T3 Control presentation cellular morphology under different fluorescent filters using DAPI (blue), AO (green), PI (red), and merged filter. ((A) ×100, scale bar 20 µm (B) ×20, scale bar 100 µm).

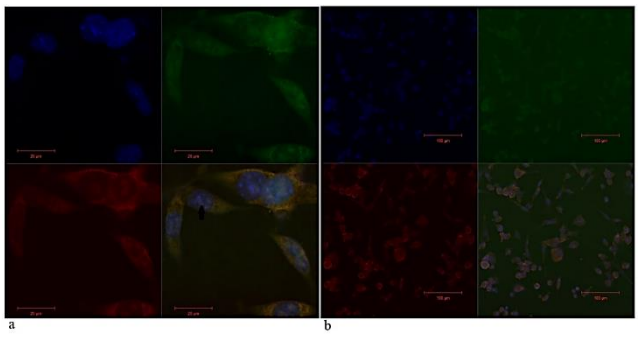

Figure 9: Confocal micrographs of Au-CsCaCO3NPs treated NIH3T3 cells presentation cellular acceptance and morphology under different fluorescent filters using DAPI (blue), AO (green), PI (red) and merged filter (living cells (control cells) pointer by black arrow). ((A) ×100, scale bar 20 µm (B) ×20, scale bar 100 µm).

Discussion

The results show a biocompatibility assessment of the nanoparticles on the cell lines by evaluating the cell membrane integrity. It was initially established that a normal cell membrane is impermeable to LDH release activity, and a common and standard biocompatibility test was used in *in vitro* cytotoxicity studies (57). A bioassay was used to quantify the number of dead cells through LDH leaked from the damaged cell plasma membrane correlating to cell death rate (59). This study surprisingly illustrates that the conjugated nanoparticles LDH % release of NIH3T3 was significantly lower compared to that of MCF-7. This result could be clarified because nanoparticle internalization could prompt intracellular responses along with the growing accumulation of LDH within the cytosol, facilitating the reverse conversion of lactate to pyruvate following a decrease of NAD^+ to NADH within the cell. Furthermore, these results propose the possibility of conjugated particles for biomolecular and cellular bio-medical uses, such as imaging and drug distribution.

Several reports have proven LDH to oxidize lactate to pyruvate while consuming NADH (60). The cytosolic enzymes are released into the extracellular liquids only when the cell membrane integrity is absent, assessing the cell membrane integrity by calculating the quantity of LDH released from the lysed cells, which is directly proportional to the damaged cells (58). Recent literature on LDH findings with work done on cancer cell line HeLa and MCF-7 using nanoparticle delivery systems and surface functionalized nanoparticles have reported higher LDH leakages (61). In the same regard, high LDH leakages have been confirmed with MCF-7 as a result of metallic nanoparticles (62), but also known reports have argued that lower LDH release with slight comprises of the cell membrane integrity by fibroblast cells L929 (63). However, this outcome is contrary to that of Smith (58), Lanari (64), Abdullah (65), Koren (66) who found that LDH assay studies on HeLa, MCF-7, and NIH3T3 using gold nanoribbons revealed utmost LDH discharge in HeLa than MCF-7 and reported no significant difference with the LDH% discharge between MCF-7 and NIH3T3 (67). In addition, previous studies on nanomaterials have reported that they induce high LDH levels, attributed to nanoparticle morphology inducing oxidative stress (68). Therefore, the current LDH results revealed no toxicity, as demonstrated by the conjugated nanoparticles.

Collectively, the overall ROS assay findings of the nanoparticles on MCF-7 and NIH3T3 offer beneficial thought into O_2 metabolism. ROS refers to chemicals, radicals, or molecules that include reactive oxygen composites, for example, peroxides subsequent from typical O_2 metabolism with vigorous characters in homeostasis and cell signaling (69). This study was intended to determine the cell lines' relative fluorescence units (RFU). The results in this work indicate that the Au-$CsCaCO_3$NPs treated MCF-7 cells showed greater ROS release as paralleled to the Au-$CsCaCO_3$NPs treated NIH3T3 cells. ROS generation of the NIH3T3 was considerably lesser than on MCF-7 and showed reliable ROS generation, likewise in agreement with earlier biocompatibility outcomes highlighting the remarkability of Au-$CsCaCO_3$NPs.

Consequently, these outcomes could be explained by the statement that the internalization of the nanoparticles probably caused oxidative stress, which, in sequence, caused cell death, as displayed in the outcomes. This work supports evidence that the introduction of environmental stress significantly raises ROS levels, producing considerable cellular injury, furthermore, known as oxidative stress (70). Also, it corroborates the results of earlier studies in which cancer cells create significant levels of ROS. This is further explained by increased metabolic activities of oxidases and peroxisomes, mitochondria malfunctioning, or cellular dysfunction (71-73). Constant with prior works, this research found literature that reported nanoparticle cellular acceptance to make mitochondrial membrane penetrability and damaging the respiratory chain, producing apoptosis (74). Similarly, it has been argued for native cancer treatment that (Burkitt lymphoma B cells) and (epithelial breast cancer cells) produced probable injury using directed X-ray and AuNPs causing great ROS generation leading to cellular necrosis or apoptosis nonetheless, whereas supporting slight injury to neighboring, particle-free tissue (75).

Furthermore, it has been proven that carbon and metallic nanomaterials produce slight ROS. But, their morphology, size, positive surface charges, aggregation, cellular interface, and nano metallic ions guide oxidative stress discharge, producing physiological dysfunction of the cell, which in sequence stimulates DNA injury (76,77). This finding contradicts previous studies, which have suggested a significantly higher generation of ROS over time by metallic nanomaterial as described by Xue (78) with works on human

liver HepG2 cells. Similarly, no significant effects were found with the work on NIH3T3 cells (79). Conclusively, these results offer competencies of the conjugated nanoparticles for cellular imaging applications.

These results provide interesting insights into fluorescence and confocal imaging of the Au-$CsCaCO_3$NPs treated cells of MCF-7 and NIH3T3 using AO, PI double staining, and DAPI. The current work was intended to define the cell death and cellular acceptance of the synthesized nanoparticles where the most prominent finding to arise from the fluorescence imaging is the fact that the MCF-7 treated cells observed more cell deaths in comparison to the NIH3T3 treated cells counterparts. Additionally, from the confocal imaging, it is abundantly clear that the cells could take up nanoparticles within their cellular compartments. These results reflect those of Feng (80) and Yuan (81), who also found that fabricated bio-conjugated nanoparticles confirmed cellular internalization into MCF-7 and MDA-MB-231 over NIH3T3. Furthermore, these results encourage agreement with further work. In this water, soluble fluorescent conjugated polyelectrolytes with self-assembly 3D nanostructures were established to use for bioimaging of cancer and normal cell lines, including MCF-7 and NIH3T3 which also showed comparable figures as well (82).

In addition, the present study also supports similar evidence from Zhang (83) that conjugated nanoparticles were booked up by the treated MCF-7 and NIH3T3 cells. More importantly, the results align with recent studies that confirmed cellular acceptance of the nanoparticles, cell death findings, and non-toxicity to the normal cell line over the cancer cell line (84-86). Although these results differ from some published studies Muehlmann (87) and Li (88) they are consistent with several recent works Li (89), Li (90) and Yang (91). It seems likely that these results could be due to a numeral of features affecting the efficiency of the nanoparticles and cellular uptake, for example, size, shape, charge, and surface modification of the nanoparticles, explained by pinocytosis, a type of endocytosis associated with internalization of the nanoparticles. Elaborately, smaller particles, such as nanoparticles, can easily be internalized by the cell (92-95). Regarding shape and charge, it has been confirmed that more positive charges and spherical particles are easily booked up by the cell caused by the highly negative charge present in the cell membrane (96-100). These are useful results; therefore, it is safe and possible that our conjugated nanoparticles could be used for bio-imaging.

Conclusions

This research aimed to assess fluorescent imaging and bio-cellular uptake of the Au-CsCaCO3NPs. Based on the results of this study, it is now possible to state that the easily synthesized conjugated nanoparticles are biocompatible, environmentally friendly, and could be used for bio-imaging. Moreover, they allowed for cellular uptake by cancer cells and standard cells and imparted cell death to the cancer cells in contrast to the standard cells. Altogether, these findings recommend the possible opportunity the synthesized conjugated nanoparticles could play in progressing cancer imaging. This research extends our knowledge of bio-imaging using Au-CsCaCO3NPs and its potential application in diseased-cellular diagnostics.

Conflict of interests

The authors announce that they have no competing interests in the publication of this research article.

Acknowledgments

We would like to thank all the staff of (Institute of Bioscience, Universiti Putra Malaysia), and (Department of Veterinary Preclinical Sciences, Faculty of Veterinary Medicine, Universiti Putra Malaysia) who assisted in obtaining the data. This work is financially supported by Fundamental Research Grant Scheme (FRGS) provided by Malaysian Government [Grant Project no. 5524842] and Islamic Development Bank M.Sc. Scholarship Programme.

References

1. Guo D, Xie G, Luo J. Mechanical properties of nanoparticles: Basics and applications. J Phys D Appl Phys. 2013;47(1):013001. DOI: 10.1088/0022-3727/47/1/013001
2. Jamal SA. Application of nanoparticles of ceramics, peptides, silicon, carbon, and diamonds in tissue engineering. Chem Sci J. 2013;4(1):1. [available at]
3. van Rijt S, Habibovic P. Enhancing regenerative approaches with nanoparticles. J R Soc Interface. 2017;14(129):20170093. DOI: 10.1098/rsif.2017.0093
4. Wang R, Lang J, Liu Y, Lin Z, Yan X. Ultra-small, size-controlled Ni (OH) 2 nanoparticles: Elucidating the relationship between particle size and electrochemical performance for advanced energy storage devices. NPG Asia Mater. 2015;7(6):e183. DOI: 10.1038/am.2015.42
5. Kong FY, Zhang JW, Li RF, Wang ZX, Wang WJ, Wang W. Unique roles of gold nanoparticles in drug delivery, targeting and imaging applications. Molecules. 2017;22(9):1445. DOI: 10.3390/molecules22091445
6. Kenry WC, Loh KP, Lim CT. When stem cells meet graphene: Opportunities and challenges in regenerative medicine. Biomaterials. 2018;155:236-250. DOI: 10.1016/j.biomaterials.2017.10.004
7. Volkova N, Pavlovich O, Fesenko O, Budnyk O, Kovalchuk S, Goltsev A. Studies of the influence of gold nanoparticles on characteristics of mesenchymal stem cells. J Nanomater. 2017;2017:9. DOI: 10.1155/2017/6934757
8. De Silva RT, Mantilaka MM, Goh KL, Ratnayake SP, Amaratunga GA, de Silva KM. Magnesium oxide nanoparticles reinforced electrospun alginate-based nanofibrous scaffolds with improved physical properties. Int J Biomater. 2017;2017:9. DOI: 10.1155/2017/1391298
9. Walmsley GG, McArdle A, Tevlin R, Momeni A, Atashroo D, Hu MS, Feroze AH, Wong VW, Lorenz PH, Longaker MT, Wan DC. Nanotechnology in bone tissue engineering. Nanomed Nanotech Biol Med. 2015;11(5):1253-1263. DOI: 10.1016/j.nano.2015.02.013
10. Naser AI, Hamed RS, Taqa GA. The impact of silver/beta-tricalcium phosphate nanocomposite combined with injectable platelet-rich fibrin on the healing of mandibular bone defects: An experimental study in

Dogs. Iraqi J Vet Sci. 2024;38(3):501-507. DOI: 10.33899/ijvs.2024.145856.3400
11. Atiyah AG, Alkattan LM, Shareef AM. The radiological study of using fabricated calcium hydroxide from quail eggshell and plasma-rich fibrin for reconstitution of a mandibular bone gap in dogs. Iraqi J Vet Sci. 2024;38(1):55-62. DOI: 10.33899/ijvs.2023.139898.2998
12. Bader OA, Jasim AM, Jawad MJ, Nahi HH. The role of PLGA/TPGS nanoparticle on xylazine-ketamine anesthetic activity in male albino rabbits. Iraqi J Vet Sci. 2022;36(1):201-206. DOI: 10.33899/ijvs.2021.129688.1679
13. Al-Zubaidi MR, Thwiny HT, Al-Biati MN. Modulation of chitosan nanoparticles properties for sheep pox mucosal vaccine delivery with cytotoxicity and release Studies-*in vitro*. Iraqi J Vet Sci. 2023;37(I-IV):111-119. DOI: 10.33899/ijvs.2023.1374030.2682
14. Al-Murshidi MM, Khadhim IA, Al-Mafragy HS. Evaluation of the antidiabetic activity of zinc oxide and chromium oxide nanoparticles alone or in combination on the pancreas of alloxan-induced diabetes mellitus in male albino mice (*Mus musculus*). Iraqi J Vet Sci. 2023;37(I-IV):159-163. DOI: 10.33899/ijvs.2023.138380.2797
15. Chapman S, Dobrovolskaia M, Farahani K, Goodwin A, Joshi A, Lee H, Meade T, Pomper M, Ptak K, Rao J, Singh R. Nanoparticles for cancer imaging: The good, the bad, and the promise. Nano Today. 2013;8(5):454-460. DOI: 10.1016/j.nantod.2013.06.001
16. Baetke SC, Lammers TG, Kiessling F. Applications of nanoparticles for diagnosis and therapy of cancer. Br J Radiol. 2015;88(1054):20150207. DOI: 10.1259/bjr.20150207
17. Jaji AZ, Zakaria ZA, Mahmud R, Loqman MY, Hezmee MN, Abba Y, Isa T, Mahmood SK. Safety assessments of subcutaneous doses of aragonite calcium carbonate nanocrystals in rats. J Nanoparticle Res. 2017;19:1-8. DOI: 10.1007/s11051-017-3849-z
18. Nicolardi S, Van Der Burgt YE, Codée JD, Wuhrer M, Hokke CH, Chiodo F. Structural characterization of biofunctionalized gold nanoparticles by ultrahigh-resolution mass spectrometry. ACS Nano. 2017;11(8):8257-8264. DOI: 10.1021/acsnano.7b03402
19. Shafiu Kamba A, Zakaria ZA. Osteoblasts growth behaviour on bio-based calcium carbonate aragonite nanocrystal. Biomed Res Int. 2014;2014. DOI: 10.1155/2014/215097
20. Gao Y, Sun Y, Zou H, Sheng Y, Zhou X, Zhang B, Zhou B. Effect of Eu3+ doping on the structural and photoluminescence properties of cubic CaCO3. Mater Sci Eng B Solid-State Mater Adv Technol. 2016;203:52-58. DOI: 10.1016/j.mseb.2015.09.004
21. Yan M, Zou H, Zhao H, Song Y, Zheng K, Sheng Y, Wang G, Huo Q. Fabrication and photoluminescence properties of TiO 2: Eu 3+ microspheres with tunable structure from solid to core–shell. Cryst Eng Comm. 2014;16(39):9216-9223. DOI: 10.1039/C4CE01048E
22. Xie Y, Ma S, Wang Y, Xu M, Lu C, Xiao L, Deng S. Controlled synthesis and luminescence properties of CaMoO4: Eu^{3+} microcrystals. Optical Mater. 2018;77:13-18. DOI: 10.1016/j.optmat.2018.01.015
23. Biswas A, Nagaraja AT, McShane MJ. Fabrication of nanocapsule carriers from multilayer-coated vaterite calcium carbonate nanoparticles. ACS Appl Mater Interfaces. 2014;6(23):21193-21201. DOI: 10.1021/am5061195
24. Khalil I, Julkapli NM, Yehye WA, Basirun WJ, Bhargava SK. Graphene–gold nanoparticles hybrid—synthesis, functionalization, and application in an electrochemical and surface-enhanced raman scattering biosensor. Materials. 2016;9(6):406. DOI: 10.3390/ma9060406
25. Abdolmohammadi S, Siyamak S, Ibrahim NA, Yunus WM, Rahman MZ, Azizi S, Fatehi A. Enhancement of mechanical and thermal properties of polycaprolactone/chitosan blend by calcium carbonate nanoparticles. Int J Mol Sci. 2012;13(4):4508-4522. DOI: 10.3390/ijms13044508
26. Muxika A, Etxabide A, Uranga J, Guerrero P, De La Caba K. Chitosan as a bioactive polymer: Processing, properties and applications. Int J Biol Macromol. 2017;105:1358-1368. DOI: 10.1016/j.ijbiomac.2017.07.087
27. Capek I. Polymer decorated gold nanoparticles in nanomedicine conjugates. Adv Colloid Interface Sci. 2017;249:386-399. DOI: 10.1016/j.cis.2017.01.007
28. Dziawer L, Koźmiński P, Męczyńska-Wielgosz S, Pruszyński M, Łyczko M, Wąs B, Celichowski G, Grobelny J, Jastrzębski J, Bilewicz A. Gold nanoparticle bioconjugates labelled with 211 At for targeted alpha therapy. RSC Adv. 2017;7(65):41024-41032. DOI: 10.1039/C7RA06376H
29. Kairdolf BA, Qian X, Nie S. Bioconjugated nanoparticles for biosensing, in vivo imaging, and medical diagnostics. Anal Chem. 2017;89(2):1015-1031. DOI: 10.1021/acs.analchem.6b04873
30. Uchiyama MK, Deda DK, Rodrigues SF, Drewes CC, Bolonheis SM, Kiyohara PK, Toledo SP, Colli W, Araki K, Farsky SH. In vivo and in vitro toxicity and anti-inflammatory properties of gold nanoparticle bioconjugates to the vascular system. Toxicol Sci. 2014;142(2):497-507. DOI: 10.1093/toxsci/kfu202
31. Singh R, Patil S, Singh N, Gupta S. Dual functionality nanobioconjugates targeting intracellular bacteria in cancer cells with enhanced antimicrobial activity. Sci Rep. 2017;7(1):5792. DOI: 10.1038/s41598-017-06014-4
32. Kapur A, Aldeek F, Ji X, Safi M, Wang W, Del Cid A, Steinbock O, Mattoussi H. Self-assembled gold nanoparticle–fluorescent protein conjugates as platforms for sensing thiolate compounds via modulation of energy transfer quenching. Bioconjug Chem. 2017;28(2):678-687. DOI: 10.1021/acs.bioconjchem.7b00006
33. Hondred JA, Breger JC, Garland NT, Oh E, Susumu K, Walper SA, Medintz IL, Claussen JC. Enhanced enzymatic activity from phosphotriesterase trimer gold nanoparticle bioconjugates for pesticide detection. Analyst. 2017;142(17):3261-3271. [available at]
34. Xing R, Jiao T, Yan L, Ma G, Liu L, Dai L, Li J, Möhwald H, Yan X. Colloidal gold–collagen protein core–shell nanoconjugate: One-step biomimetic synthesis, layer-by-layer assembled film, and controlled cell growth. ACS Appl Mater Interfaces. 2015;7(44):24733-24740. DOI: 10.1021/acsami.5b07453
35. Del Caño R, Mateus L, Sánchez-Obrero G, Sevilla JM, Madueño R, Blázquez M, Pineda T. Hemoglobin bioconjugates with surface-protected gold nanoparticles in aqueous media: The stability depends on solution pH and protein properties. J Colloid Interface Sci. 2017;505:1165-1171. DOI: 10.1016/j.jcis.2017.07.011
36. Huang X, Jain PK, El-Sayed IH, El-Sayed MA. Plasmonic photothermal therapy (PPTT) using gold nanoparticles. Lasers Med Sci. 2008;23:217-228. DOI: 10.1007/s10103-007-0470-x
37. Boisselier E, Astruc D. Gold nanoparticles in nanomedicine: Preparations, imaging, diagnostics, therapies, and toxicity. Chem Soc Rev. 2009;38(6):1759-1782. DOI: 10.1039/B806051G
38. Dreaden EC, Austin LA, Mackey MA, El-Sayed MA. Size matters gold nanoparticles in targeted cancer drug delivery. Ther Deliv. 2012;3(4):457-478. DOI: 10.4155/tde.12.21
39. Anselmo AC, Mitragotri S. Nanoparticles in the clinic. Bioeng Transl Med. 2016;1(1):10-29. DOI: 10.1002/btm2.10003
40. Yeh YC, Creran B, Rotello VM. Gold nanoparticles: Preparation, properties, and applications in bionanotechnology. Nanoscale. 2012;4(6):1871-1880. DOI: 10.1039/C1NR11188D
41. Calixto GM, Bernegossi J, De Freitas LM, Fontana CR, Chorilli M. Nanotechnology-based drug delivery systems for photodynamic therapy of cancer: A review. Molecules. 2016;21(3):342. DOI: 10.3390/molecules21030342
42. Wei J, Niikura K, Higuchi T, Kimura T, Mitomo H, Jinnai H, Joti Y, Bessho Y, Nishino Y, Matsuo Y, Ijiro K. Yolk/Shell assembly of gold nanoparticles by size segregation in solution. J Am Chem Soc. 2016;138(10):3274-3277. DOI: 10.1021/jacs.5b12456
43. Lisha KP, Anshup, Pradeep T. Enhanced visual detection of pesticides using gold nanoparticles. J Environ Sci Health B. 2009;44(7):697-705. DOI: 10.1080/03601230903163814
44. Inbaraj BS, Chen BH. Nanomaterial-based sensors for detection of foodborne bacterial pathogens and toxins as well as pork adulteration in meat products. J Food Drug Anal. 2016;24(1):15-28. DOI: 10.1016/j.jfda.2015.05.001
45. Gao Y, Liu L, Shen B, Chen X, Wang L, Wang L, Feng W, Huang C, Li F. Amphiphilic PEGylated lanthanide-doped upconversion nanoparticles for significantly passive accumulation in the peritoneal metastatic carcinomatosis models following intraperitoneal

administration. ACS Biomater Sci Eng. 2017;3(9):2176-2184. DOI: 10.1021/acsbiomaterials.7b00416
46. Li SD, Huang L. Pharmacokinetics and biodistribution of nanoparticles. Mol Pharm. 2008;5(4):496-504. DOI: 10.1021/mp800049w
47. Petros RA, DeSimone JM. Strategies in the design of nanoparticles for therapeutic applications. Nat Rev Drug Discov. 2010;9(8):615-627. [available at]
48. Markman JL, Rekechenetskiy A, Holler E, Ljubimova JY. Nanomedicine therapeutic approaches to overcome cancer drug resistance. Adv Drug Deliv Rev. 2013;65(13-14):1866-1879. DOI: 10.1016/j.addr.2013.09.019
49. Jain RK. Transport of molecules, particles, and cells in solid tumors. Annu Rev Biomed Eng. 1999;1(1):241-263. DOI: 10.1146/annurev.bioeng.1.1.241
50. Verhoef JJ, Anchordoquy TJ. Questioning the use of PEGylation for drug delivery. Drug Deliv Transl Res. 2013;3:499-503. DOI: 10.1007/s13346-013-0176-5
51. Peng H, Li K, Wang T, Wang J, Wang J, Zhu R, Sun D, Wang S. Preparation of hierarchical mesoporous CaCO 3 by a facile binary solvent approach as anticancer drug carrier for etoposide. Nanoscale Res Lett. 2013;8:1-10. DOI: 10.1186/1556-276X-8-321
52. Lammers TG, Hennink WE, Storm G. Tumour-targeted nanomedicines: Principles and practice. Br J Cancer. 2008;99(3):392-397. DOI: 10.1038/sj.bjc.6604483
53. Huang HC, Barua S, Sharma G, Dey SK, Rege K. Inorganic nanoparticles for cancer imaging and therapy. J Control Release. 2011;155(3):344-357. DOI: 10.1016/j.jconrel.2011.06.004
54. Maeda H, Wu J, Sawa T, Matsumura Y, Hori K. Tumor vascular permeability and the EPR effect in macromolecular therapeutics: A review. J Control Release. 2000;65(1-2):271-284. DOI: 10.1016/S0168-3659(99)00248-5
55. Turkevich J, Stevenson PC, Hiller J. Synthesis of gold nanoparticles Turkevich method. Discuss Faraday Soc. 1951;11:55-75. [available at]
56. Kiranda HK, Mahmud R, Abubakar D, Zakaria ZA. Fabrication, characterization, and cytotoxicity of spherical-shaped conjugated gold-cockle shell derived calcium carbonate nanoparticles for biomedical applications. Nanoscale Res Lett. 2018;13:1-10. DOI: 10.1186/s11671-017-2411-3
57. Allen M, Millett P, Dawes E, Rushton N. Lactate dehydrogenase activity as a rapid and sensitive test for the quantification of cell numbers in vitro. Clin Mater. 1994;16(4):189-194. DOI: 10.1016/0267-6605(94)90116-3
58. Smith SM, Wunder MB, Norris DA, Shellman YG. A simple protocol for using an LDH-based cytotoxicity assay to assess the effects of death and growth inhibition at the same time. PLoS One. 2011;6(11):e26908. DOI: 10.1371/journal.pone.0026908
59. Khattak SF, Spatara M, Roberts L, Roberts SC. Application of colorimetric assays to assess viability, growth, and metabolism of hydrogel-encapsulated cells. Biotechnol Lett. 2006;28:1361-1370. DOI: 10.1007/s10529-006-9104-9
60. Legrand C, Bour JM, Jacob C, Capiaumont J, Martial A, Marc A, Wudtke M, Kretzmer G, Demangel C, Duval D, Hache J. Lactate dehydrogenase LDH activity of the number of dead cells in the medium of cultured eukaryotic cells as marker. J Biotechnol. 1992;25(3):231-243. DOI: 10.1016/0168-1656(92)90158-6
61. Chowdhury SM, Xie S, Fang J, Lee SK, Sitharaman B. Nanoparticle-facilitated membrane depolarization-induced receptor activation: implications on cellular uptake and drug delivery. ACS Biomater Sci Eng. 2016;2(12):2153-2161. DOI: 10.1021/acsbiomaterials.6b00338
62. Elshawy OE, Helmy EA, Rashed LA. Preparation, characterization, and in vitro evaluation of the antitumor activity of the biologically synthesized silver nanoparticles. Adv Nanoparticles. 2016;5(02):149-166. [available at]
63. Gurunathan S, Han JW, Eppakayala V, Jeyaraj M, Kim JH. Cytotoxicity of biologically synthesized silver nanoparticles in MDA-MB-231 human breast cancer cells. Biomed Res Int. 2013;2013:10. DOI: 10.1155/2013/535796
64. Lanari C, Lüthy I, Lamb CA, Fabris V, Pagano E, Helguero LA, Sanjuan N, Merani S, Molinolo AA. Five novel hormone-responsive cell lines derived from murine mammary ductal carcinomas: In vivo and in vitro effects of estrogens and progestins. Cancer Res. 2001;61(1):293-302. [available at]
65. Abdullah AS, Mohammed AS, Abdullah R, Mirghani ME, Al-Qubaisi M. Cytotoxic effects of *Mangifera indica* L. kernel extract on human breast cancer (MCF-7 and MDA-MB-231 cell lines) and bioactive constituents in the crude extract. BMC Complement Altern Med. 2014;14(1):1-10. DOI: 10.1186/1472-6882-14-199
66. Koren III J, Miyata Y, Kiray J, O'Leary III JC, Nguyen L, Guo J, Blair LJ, Li X, Jinwal UK, Cheng JQ, Gestwicki JE. Rhodacyanine derivative selectively targets cancer cells and overcomes tamoxifen resistance. PLoS One. 2012;7(4): e35566. DOI: 10.1371/journal.pone.0035566
67. Chowdhury SM, Lalwani G, Zhang K, Yang JY, Neville K, Sitharaman B. Cell specific cytotoxicity and uptake of graphene nanoribbons. Biomaterials. 2013;34(1):283-293. DOI: 10.1016/j.biomaterials.2012.09.057
68. Zhang Y, Ali SF, Dervishi E, Xu Y, Li Z, Casciano D, Biris AS. Cytotoxicity effects of graphene and single-wall carbon nanotubes in neural phaeochromocytoma-derived PC12 cells. ACS Nano. 2010;4(6):3181-3186. DOI: 10.1021/nn1007176
69. Seabra AB, Durán N. Nanotoxicology of metal oxide nanoparticles. Metals. 2015;5(2):934-975. DOI: 10.3390/met5020934
70. Gruhlke MC, Nicco C, Batteux F, Slusarenko AJ. The effects of allicin, a reactive sulfur species from garlic, on a selection of mammalian cell lines. Antioxidants. 2016;6(1):1. DOI: 10.3390/antiox6010001
71. Liou GY, Storz P. Reactive oxygen species in cancer. Free Radical Res. 2010;44(5):479-496. DOI: 10.3109/10715761003667554
72. Sullivan LB, Chandel NS. Mitochondrial reactive oxygen species and cancer. Cancer Metab. 2014;2:1-2. DOI: 10.1186/2049-3002-2-17
73. Szatrowski TP, Nathan CF. Production of large amounts of hydrogen peroxide by human tumor cells. Cancer Res. 1991;51(3):794-798. [available at]
74. Park EJ, Yi J, Chung KH, Ryu DY, Choi J, Park K. Oxidative stress and apoptosis induced by titanium dioxide nanoparticles in cultured BEAS-2B cells. Toxicol Lett. 2008;180(3):222-229. DOI: 10.1016/j.toxlet.2008.06.869
75. Minai L, Yeheskely-Hayon D, Yelin D. High levels of reactive oxygen species in gold nanoparticle-targeted cancer cells following femtosecond pulse irradiation. Sci Rep. 2013;3(1):2146. [available at]
76. Fu PP, Xia Q, Hwang HM, Ray PC, Yu H. Mechanisms of nanotoxicity: Generation of reactive oxygen species. J Food Drug Anal. 2014;22(1):64-75. DOI: 10.1016/j.jfda.2014.01.005
77. Saravanakumar G, Kim J, Kim WJ. Reactive-oxygen-species-responsive drug delivery systems promises and challenges. Adv Sci. 2017;4(1):1600124. DOI: 10.1002/advs.201600124
78. Xue Y, Zhang T, Zhang B, Gong F, Huang Y, Tang M. Cytotoxicity and apoptosis induced by silver nanoparticles in human liver HepG2 cells in different dispersion media. J Appl Toxicol. 2016;36(3):352-360. DOI: 10.1002/jat.3199
79. Zhang W, Hu S, Yin JJ, He W, Lu W, Ma M, Gu N, Zhang Y. Prussian blue nanoparticles as multienzyme mimetics and reactive oxygen species scavengers. J Am Chem Soc. 2016;138(18):5860-5865. DOI: 10.1021/jacs.5b12070
80. Feng G, Liu J, Geng J, Liu B. Conjugated polymer microparticles for selective cancer cell image-guided photothermal therapy. J Mater Chem B. 2015;3(6):1135-1141. DOI: 10.1039/C4TB01590H
81. Yuan Y, Feng G, Qin W, Tang BZ, Liu B. Targeted and image-guided photodynamic cancer therapy based on organic nanoparticles with aggregation-induced emission characteristics. Chem Commun. 2014;50(63):8757-8760. DOI: 10.1039/C4CC02767A
82. Pu KY, Liu B. Fluorescent conjugated polyelectrolytes for bioimaging. Adv Funct Mater. 2011;21(18):3408-3423. DOI: 10.1002/adfm.201101153
83. Zhang YH, Zhang YM, Yang Y, Chen LX, Liu Y. Controlled DNA condensation and targeted cellular imaging by ligand exchange in a polysaccharide–quantum dot conjugate. Chem Commun. 2016;52(36):6087-6090. DOI: 10.1039/C6CC01571A

التصوير التألقي وتقييم امتصاص الخلايا الحيوية لصبغة الذهب القريبة من الأشعة تحت الحمراء المصاحبة لجسيمات كربونات الكالسيوم النانوية

حنان كريمة كيراندا[١]، روزي بنتي محمود[٢]، سفانه خضر محمود[٣]، زوكي أبو بكر زكريا[٤]

[١]مركز البحث والابتكار، كلية هامبر، معهد التكنولوجيا والتعليم المتقدم، تورونتو، أونتاريو، كندا، [٢]قسم التصوير، كلية الطب والعلوم الصحية، جامعة بوترا ماليزيا، سيردانغ، ماليزيا، [٣]فرع التشريح، كلية الطب البيطري، جامعة الموصل، الموصل، العراق، [٤]قسم العلوم البيطرية قبل السريرية، كلية الطب البيطري، جامعة بوترا ماليزيا، سيردانغ، ماليزيا

الخلاصة

في السنوات الأخيرة، برز التصوير التألقي كمجال نشط للاهتمام في التصوير الطبي. يلعب التصوير التألقي دورا حاسما في التصوير الجزيئي. تشير الدلائل إلى استخدامه في توفير نظرة هيكلية مفصلة والعوامل الوراثية والخلوية لإجراءات الجسم على المستوى الجزيئي. تم تحديد عوامل التصوير على أنها مرتبطة بمخاطر مثل عدم التفكك البيولوجي والتسمم الهائل. أظهر الباحثون اهتماما شديدا بنمو العوامل المستهدفة متعددة الوظائف في علاج الأورام والتصوير التألقي بالأشعة تحت الحمراء القريبة. قيمت هذه الدراسة التصوير التألقي وتقييم امتصاص الخلايا الحيوية لصبغة الذهب القريبة من الأشعة تحت الحمراء المصاحبة لجسيمات كربونات الكالسيوم النانوية. تم دراسة خصائص الحجم والتشكل لصبغة الذهب القريبة من الأشعة تحت الحمراء المُصنَّعة والمصاحبة لجسيمات كربونات الكالسيوم النانوية بواسطة المجهر الإلكتروني النافذ، وإمكانات زيتا، ومقياس الطيف الضوئي للأشعة فوق البنفسجية. تم تقييم التوافق الحيوي لصبغة الذهب القريبة من الأشعة تحت الحمراء المُصنَّعة والمصاحبة لجسيمات كربونات الكالسيوم النانوية في خلايا سرطان الثدي البشرية المستزرعة MCF-7 والخلايا الليفية الجنينية الفأرية NIH3T3 باستخدام الاختبارات الحيوية مثل هيدروجينز اللاكتات وأنواع الأكسجين التفاعلية للفحص السمي. تمت دراسة التشكل الخلوي والامتصاص بواسطة المجهر التألقي ومتحد البؤر. أثبتت النتائج أن خلايا سرطان الثدي البشرية المستزرعة والمعالجة بصبغة الذهب القريبة من الأشعة تحت الحمراء والمصاحبة لجسيمات كربونات الكالسيوم النانوية أظهرت موت خلايا أكثر من الخلايا الليفية الجنينية الفأرية بالإضافة إلى ذلك، كانت الخلايا قادرة على تحمل الجسيمات النانوية داخل حجراتها الخلوية. في الختام، تم تصنيع صبغة الذهب القريبة من الأشعة تحت الحمراء والمصاحبة لجسيمات كربونات الكالسيوم النانوية بسهولة، وكانت متوافقة حيويا، وصديقة للبيئة. من الجدير بالذكر أنه يمكن استخدام صبغة الذهب القريبة من الأشعة تحت الحمراء والمصاحبة لجسيمات كربونات الكالسيوم النانوية للتصوير التألقي بشكل امن والذي يمكن أن يوفر فرصا للتقدم في تصوير جميع أنواع السرطانات.

84. Li K, Liu B. Polymer-encapsulated organic nanoparticles for fluorescence and photoacoustic imaging. Chem Soc Rev. 2014;43(18):6570-6597. DOI: 10.1039/C4CS00014E
85. Geng J, Li K, Pu KY, Ding D, Liu B. Conjugated polymer and gold nanoparticle co-loaded PLGA nanocomposites with eccentric internal nanostructure for dual-modal targeted cellular imaging. Small. 2012;8(15):2421-2429. DOI: 10.1002/smll.201102353
86. Li K, Jiang Y, Ding D, Zhang X, Liu Y, Hua J, Feng SS, Liu B. Folic acid-functionalized two-photon absorbing nanoparticles for targeted MCF-7 cancer cell imaging. Chem Commun. 2011;47(26):7323-7325. DOI: 10.1039/C1CC10739A
87. Muehlmann LA, Ma BC, Longo JP, Almeida Santos MD, Azevedo RB. Aluminum–phthalocyanine chloride associated to poly (methyl vinyl ether-co-maleic anhydride) nanoparticles as a new third-generation photosensitizer for anticancer photodynamic therapy. Int J Nanomed. 2014:1199-1213. [available at]
88. Li J, You J, Dai Y, Shi M, Han C, Xu K. Gadolinium oxide nanoparticles and aptamer-functionalized silver nanoclusters-based multimodal molecular imaging nanoprobe for optical/magnetic resonance cancer cell imaging. Anal Chem. 2014;86(22):11306-11311. DOI: 10.1021/ac503026d
89. Li Z, Yi PW, Sun Q, Lei H, Li Zhao H, Zhu ZH, Smith SC, Lan MB, Lu GQ. Ultrasmall water-soluble and biocompatible magnetic iron oxide nanoparticles as positive and negative dual contrast agents. Adv Funct Mater. 2012;22(11):2387-2393. DOI: 10.1002/adfm.201103123
90. Li K, Ding D, Huo D, Pu KY, Thao NN, Hu Y, Li Z, Liu B. Conjugated polymer-based nanoparticles as dual-modal probes for targeted in vivo fluorescence and magnetic resonance imaging. Adv Funct Mater. 2012;22(15):3107-3115. DOI: 10.1002/adfm.201102234
91. Yang B, Zhang X, Zhang X, Huang Z, Wei Y, Tao L. Fabrication of aggregation-induced emission based fluorescent nanoparticles and their biological imaging application: recent progress and perspectives. Mater Today. 2016;19(5):284-291. DOI: 10.1016/j.mattod.2015.11.002
92. Waleed A. Nanotechnology and agricultural nanofertilizers (review article). Mesopotamia J Agric. 2023;51(2):107-119. DOI: 10.33899/magrj.2023.140912.1248
93. Abdul-Majeed A, Al-Krad H. Influence of ginger as an antioxidant on the physiological performance of male quail stressed by hydrogen peroxide. Mesopotamia J Agric. 2023;51(1):141-151. DOI: 10.33899/magrj.2023.139269.1224
94. Sohby MK, Khalil HA, Eissa AM, Fekry WE. Influence of nano-silicon and nano-chitosan on growth, ion content, and antioxidant defense enzyme of two citrus rootstocks under salinity conditions. Mesopotamia J Agric. 2023;51(2):147-166. DOI: 10.33899/magrj.2023.179915
95. Alkhashb A, Alhaji T, Thalij K. Effectiveness of chitosan and Ag-nanoparticle films on the quality of chicken meat. Mesopotamia J Agric. 2024;52(2):14-26. DOI: 10.33899/mja.2024.145729.011337
96. Salatin S, Yari Khosroushahi A. Overviews on the cellular uptake mechanism of polysaccharide colloidal nanoparticles. J Cell Mol Med. 2017;21(9):1668-1686. DOI: 10.1111/jcmm.13110
97. Thurn KT, Brown E, Wu A, Vogt S, Lai B, Maser J, Paunesku T, Woloschak GE. Nanoparticles for applications in cellular imaging. Nanoscale Res Lett. 2007;2:430-441. DOI: 10.1007/s11671-007-9081-5
98. Al-Zubaidi MR, Thwiny HT, Al-Biati MN. Modulation of chitosan nanoparticles properties for sheep pox mucosal vaccine delivery with cytotoxicity and release Studies-in vitro. Iraqi J Vet Sci. 2023;37(I-IV):111-119. DOI: 10.33899/ijvs.2023.1374030.2682
99. Ezzeldein SA, Bayoumi Y, Eisa EF, Metwally M, Attia NE, Abd El Raouf M. Clinicopathological and imaging features of hypertrophic osteopathy in dogs. Iraqi J Vet Sci. 2022;36(4):991-997. DOI: 10.33899/ijvs.2022.132804.2133
100. Al-Hafedh SO, Cedden F, Gatea AO. The effectiveness of human SAGE medium compared to other conventional culture media on the ovine early embryonic development, *in vitro*. Iraqi J Vet Sci. 2024;38(2):349-356. DOI: 10.33899/ijvs.2024.140042.3014